PERGAMON

International Journal of Solids and Structures 40 (2003) 5063–5079

INTERNATIONAL JOURNAL OF SOLIDS and STRUCTURES

www.elsevier.com/locate/ijsolstr

Active stabilisation of a piezoelectric fiber composite shaft subject to follower load

Włodzimierz Kurnik [a,*], Piotr M. Przybyłowicz [b]

[a] *Warsaw University of Technology, Plac Politechniki 1, 00-661 Warsaw, Poland*
[b] *Warsaw University of Technology, Narbutta 84, 02-524 Warsaw, Poland*

Received 4 September 2002; received in revised form 7 January 2003

Abstract

The paper is concerned with active stabilisation of self-excited vibration of slender rotating columns subject to tangential follower forces. Such systems exhibit flutter-type instability as a result of energy transfer from rotation and to transverse motion of the shaft. There are two reasons for the instability to occur in rotating slender shafts—rotation in the presence of internal friction in the shaft material, and the follower load. The study reveals an interesting coupled effect of these parameters on the system stability as they create a concave set in which the system remains stable, and this means that one parameter neutralises influence of the other. The paper also takes up the problem of near-critical behaviour of the system. Non-linear bifurcation analysis is carried out to predict type of the self-excitation (either soft or hard), near-critical vibration amplitude and jump phenomena. In the second part of the paper a method of active stabilisation based on making use of piezoelectric fibre composites (PFC) is presented. The composites containing active fibres made of piezoceramics constitute the state-of-the-art structural materials capable of adjusting their mechanical state according to dynamic loading conditions. Some fundamentals concerning the operation of PFCs as rotating columns are given in the paper.

Keywords: Rotor; Composite; Follower load; Flutter; Bifurcation

1. Introduction

Non-conservative systems subject to follower forces attract attention of numerous researchers acting in the field of applied mechanics. The first to initiate the investigations was Beck (1959), who showed that an excessive compressive load applied tangentially to a cantilever results in transverse vibration of the system.

The classically formulated Beck's and Leipholz's (1972, 1980) problems have undergone various modifications. A non-uniform undamped beam with an elastic intermediate support was examined by De Rosa and Franciosi (1990), who found that the loss of stability could take place via flutter or divergence. Other works revealed that slender columns could exhibit flutter under a follower loading even when it is tensile. The key factor for the instability to occur in such a case is the presence of internal friction in the column

* Corresponding author. Fax: +48-22-660-7902.
E-mail address: wku@rekt.pw.edu.pl (W. Kurnik).

0020-7683/$ - see front matter © 2003 Elsevier Ltd. All rights reserved.
doi:10.1016/S0020-7683(03)00255-5

material. Altman and Goncalves de Oliveira (1990) presented an analysis of vibration and stability of shell panels assuming slight internal damping. The dynamic loss of stability brought about by distributed follower forces is also known to concern plates in a supersonic gas flow or pipes conveying fluids, see Païdoussis (1993). A non-linear damped Leipholz column was examined by Kurnik and Pękalak (1992), who observed near-critical behaviour of the system and formulated periodic solutions to the discovered limit cycles. They showed that tensile follower load always entails a supercritical Hopf's bifurcation, whereas compression can generate either super- or subcritical bifurcation, leading to a catastrophic loss of the equilibrium stability. Kurnik and Przybyłowicz (1995) looked for a solution to the problem of destructive subcritical bifurcation and indicated a method of prevention by making use of piezoelectric materials. It turned out that application of polymer-based piezoelectric actuators widens the stability domain and enlarges the area in which the bifurcation still preserves as supercritical.

An extended problem of the stability of Leipholz's slender column, with an additional effect taken into account, i.e. its rotation was studied by Kurnik and Przybyłowicz (2001). Any flexible rotor with permanent energy supply maintaining a constant rotation speed starts to exhibit orbital motion of its deflected form around the axis placed between the supports. This phenomenon appears at a certain angular velocity, and the necessary condition is, like in the case of non-rotating columns subject to tensile tangential force, the presence of internal damping. The two sources of the instability, i.e. follower load and rotation are different in nature, and their interaction presents an interesting dynamic problem. Both effects treated separately have been recognised more or less thoroughly but studying their combination is still an interesting challenge to be met.

This paper is concerned with an extension of that problem. It is the active stabilisation of a slender rotating column undergoing a follower load. The stabilisation is based on making use of piezoelectric elements in the form of fibres immersed in a matrix material.

The integration of piezoceramic (PZT) fibres within composite materials represents a new type of structural materials. Tiny PZT fibres of 30 μm in diameter can be aligned in an array, electrodised and then integrated into planar architectures. Such architectures are embedded within glass or graphite fibre-reinforced polymers and become piezoelectric after being poled, see Sporn and Schoencker (1999). The idea of combining piezoceramics with polymers occurred in the 1980s, see Newnham et al. (1980) and several years later it evolved towards smart composite materials. Piezoelectric fibre composites (PFCs) have a large potential for controlling. Bent et al. (1995) underlined that matrix and ceramic combinations, volume fractions, and ply angles contribute to the tailorability of PFCs, which make them applicable to structures requiring highly distributed actuation and sensing. Manufacturing technologies of PFCs have been adopted from graphite/epoxy manufacturing methods. Today, PFCs are being equipped with an interdigitated electrode pattern (the so-called IDEPFCs), see Bent and Hagood (1997). Regardless of the electrode arrangement the piezoelectric composites create a class of active materials that can cover entire structures—the actuators that are conformable to curved elements such as shafts, tubes or shells.

2. Formulation of the problem

Consider a slender rotating shaft supported on a bearing attached to one of its ends. The angular velocity ω is assumed constant, the shaft is transversely unloaded (it rotates around the vertical axis or the gravity force is neglected) but undergoes either tensile or compressive tip-concentrated follower load P—see Fig. 1. The shaft is a thin-walled structure made of a piezoelectric fibre multi-layer angle-ply composite material. The material is assumed to possess some dissipative properties. In the analysed system the damping capability of a single lamina is reflected by Kelvin–Voigt's rheological model. Additionally, certain viscous resistance from the surrounding environment, in which the column can vibrate, is also included in the analysis. The external damping will be assumed viscous. It is clear that detailed modelling of the considered thin-walled tube must result in coupled partial differential equations describing mutually

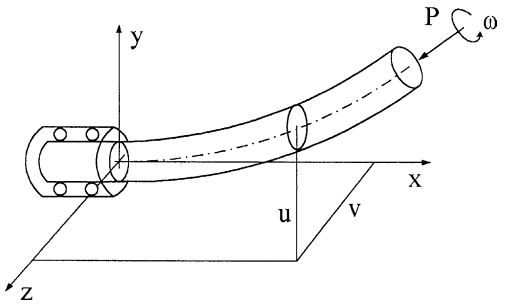

Fig. 1. Model of the rotating column.

dependent effects of bending, twisting and swelling. However, the flutter instability is related to the bending mode only, displaying the lowest natural eigenfrequency in the whole spectrum. Therefore, it is reasonable to decouple the bending mode at the level of modelling and focus the attention on the transverse vibration of the structure as a rotating beam. Additionally, having neglected the rotary and longitudinal inertia as well as the shear effect of the column, one finds the linearised equations of motion in the following form, see Kurnik and Przybyłowicz (2001):

$$\rho A\frac{\partial^2 u}{\partial t^2}+\gamma\frac{\partial u}{\partial t}+YJ\left\{\left(1+\beta\frac{\partial}{\partial t}\right)\left\{\frac{\partial^4 u}{\partial x^4}\left[\left(\frac{\partial u}{\partial x}\right)^2-1\right]+3\left(\frac{\partial^2 u}{\partial x^2}\right)^3+8\frac{\partial u}{\partial x}\frac{\partial^2 u}{\partial x^2}\frac{\partial^3 u}{\partial x^3}\right\}+\beta\omega\frac{\partial^4 v}{\partial x^4}\right\}$$
$$-\mu\frac{\partial^2 u}{\partial x^2}\left\{(1-x)\frac{\partial^2 u}{\partial x^2}-\frac{1}{2}\int_x^1\left(\frac{\partial u}{\partial\xi}\right)^2 d\xi\right\}+\frac{\partial^2 M_Z^A}{\partial x^2}=0 \tag{1}$$

$$\rho A\frac{\partial^2 v}{\partial t^2}+\gamma\frac{\partial v}{\partial t}+YJ\left\{\left(1+\beta\frac{\partial}{\partial t}\right)\left\{\frac{\partial^4 v}{\partial x^4}\left[\left(\frac{\partial v}{\partial x}\right)^2-1\right]+3\left(\frac{\partial^2 v}{\partial x^2}\right)^3+8\frac{\partial v}{\partial x}\frac{\partial^2 v}{\partial x^2}\frac{\partial^3 v}{\partial x^3}\right\}-\beta\omega\frac{\partial^4 u}{\partial x^4}\right\}$$
$$-\mu\frac{\partial^2 v}{\partial x^2}\left\{(1-x)\frac{\partial^2 v}{\partial x^2}-\frac{1}{2}\int_x^1\left(\frac{\partial v}{\partial\xi}\right)^2 d\xi\right\}+\frac{\partial^2 M_Y^A}{\partial x^2}=0 \tag{2}$$

where u and v are the transverse displacements of the shaft, β and γ are the dimensionless coefficients of the internal and external damping, respectively, ω is the rotation speed of the column, μ is the follower load, YJ is the bending stiffness, ρA is the mass density per unit length, M_Y^A and M_Z^A are the bending moments generated by active piezoelectric fibres embedded in the composite structure. Non-linear terms in Eqs. (1) and (2) appear because of the curvature of deflected equilibrium position of the rotating column during vibration. The exact relationship for the curvature has been expanded into a power series with respect to u and v, and then truncated at terms of the third order (the first non-linear approximation).

As mentioned in the introduction, the system behaviour is particularly sensitive to the damping coefficient characterising the internal friction of the column material. Consider now the stiffness matrix of the composite lamina corresponding to a plane stress–strain state expressed in the principal anisotropy axes:

$$\mathbf{Q}^*=\begin{bmatrix}\dfrac{Y_{11}\left(1+\beta_{11}\frac{\partial}{\partial t}\right)}{1-\nu_{12}^2\frac{Y_{22}}{Y_{11}}} & \dfrac{\nu_{12}Y_{22}\left(1+\beta_{22}\frac{\partial}{\partial t}\right)}{1-\nu_{12}^2\frac{Y_{22}}{Y_{11}}} & 0\\ \dfrac{\nu_{12}Y_{22}\left(1+\beta_{22}\frac{\partial}{\partial t}\right)}{1-\nu_{12}^2\frac{Y_{22}}{Y_{11}}} & \dfrac{Y_{22}\left(1+\beta_{22}\frac{\partial}{\partial t}\right)}{1-\nu_{12}^2\frac{Y_{22}}{Y_{11}}} & 0\\ 0 & 0 & G_{12}\left(1+\beta_{12}\dfrac{\partial}{\partial t}\right)\end{bmatrix} \tag{3}$$

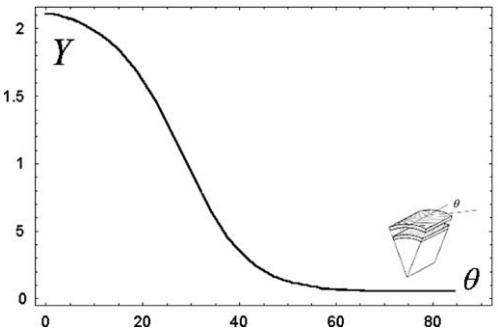

Fig. 2. Young's modulus vs. lamination angle θ.

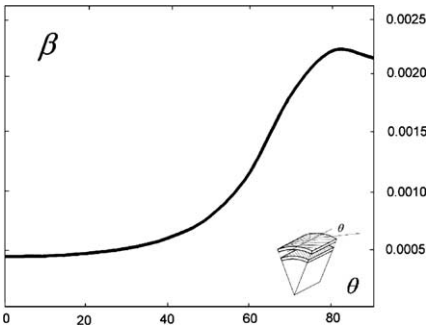

Fig. 3. Dimensional damping β vs. lamination angle θ.

The equivalent global Young's modulus of the laminate is

$$Y^* = Q_{11}^* - \frac{(Q_{12}^*)^2}{Q_{22}^*} \tag{4}$$

In fact, the global Young's modulus is, mathematically, a rational function, in which a second-degree polynomial with respect to the operator $\partial/\partial t$ stands in the numerator and a first-degree one in the denominator. Simplifying the thus determined modulus so that its form could be analogous to the mathematical formulation of Kelvin–Voigt's rheological model one finally gets

$$Y^* = Y\left(1 + \beta\frac{\partial}{\partial t}\right) \tag{5}$$

where

$$\begin{aligned} \beta &= Y_{11}\beta_{11}\cos^4\theta + Y_{22}\beta_{22}\sin^2\theta(\sin^2\theta + 2\nu_{12}\cos^2\theta) + G_{12}\beta_{12}\sin^2 2\theta \\ Y &= Y_{11}\cos^4\theta + Y_{22}\sin^2\theta(\sin^2\theta + 2\nu_{12}\cos^2\theta) + G_{12}\sin^2 2\theta \end{aligned} \tag{6}$$

Both, the resulting damping and stiffness coefficients are strongly depend on the lamination angle θ. Exemplary diagrams disclosing these quantities as functions of the ply angle are shown in Figs. 2 and 3, where typical values of β_{11}, β_{22} and β_{12} corresponding to graphite/epoxy composites were used in the calculations. It should be emphasised, however, that these values can be easily adjusted (e.g. increased) in case if needed by employing other laminae based on polymer matrices with more pronounced dissipative properties.

3. Stability of the system

As the flutter-type instability is a two-dimensional-definite phenomenon the equations of motion can be simplified by projecting their exact solution onto a subspace stretched over two, at least, approximation functions. In other words, the two partial differential equations, see Eq. (1), can be transformed into a set of four second-order ordinary differential equations by making use of bimodal Galerkin's discretisation based on the two first eigenfunctions $F_1(x)$, $F_2(x)$ corresponding to the cantilever:

$$u(x,t) = y_1(t)F_1(x) + y_2(t)F_2(x), \quad v(x,t) = z_1(t)F_1(x) + z_2(t)F_2(x) \tag{7}$$

The discretisation imposing the following orthogonality condition:

$$\int_0^1 \Gamma_i\{u[y_1(t), y_2(t), F_1(x), F_2(x)], v[z_1(t), z_2(t), F_1(x), F_2(x)]\}\mathrm{d}F_i(x) = 0, \quad i = 1, 2 \tag{8}$$

where Γ_i represents the left-hand side of the equations of motion, yields second-order ordinary differential equations, which can be then transformed into eight first-order ones by introducing new variables: $w_1 = y_1$, $w_2 = \mathrm{d}y_1/\mathrm{d}t$, $w_3 = y_2$, $w_4 = \mathrm{d}y_2/\mathrm{d}t$, $w_5 = z_1$, $w_6 = \mathrm{d}z_1/\mathrm{d}t$, $w_7 = z_2$, $w_8 = \mathrm{d}z_2/\mathrm{d}t$. The equation of motion can be now written in a compact vector form:

$$\dot{\mathbf{w}} = \mathbf{A}(\beta, \gamma, \mu, \omega)\mathbf{w} + \mathbf{N}(\mathbf{w}, \beta, \mu) \tag{9}$$

where $\mathbf{A}$ is the matrix of linearised equations and $\mathbf{N}$ represents the non-linear part. Solving the eigenvalue problem of the linearised system matrix, one obtains eight complex eigenvalues. The most interesting is the behaviour of that one with the maximum real part (r_m) as it determines the threshold of the flutter instability. The trajectory of r_m on the complex plane for increasing tensile and compressive follower load can be quite complicated, as shown in Fig. 4. It suggests that the stability region on the two-parameter plane defined by rotation speed and follower load can be concave. This can be seen in Fig. 5, where the stability region is presented for different values of the internal friction. Both these effects, i.e. μ and ω, taken separately are known to destabilise slender columns but the main intention of the investigation has been focused on the interaction between them when acting simultaneously. Unlike expected, the stability domain is not a convex set, which would have meant a synergetic effect of μ and ω. It turns out that the rotation and follower load contradict each other eventually stabilising the system, hence the set of stable combinations of μ and ω is concave.

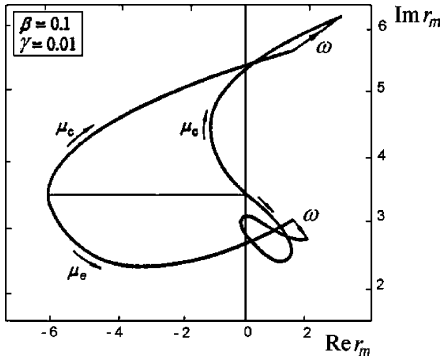

Fig. 4. Trajectory of the decisive eigenvalue.

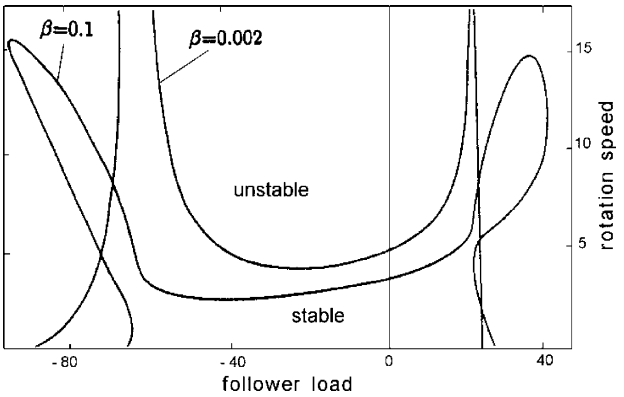

Fig. 5. Stability regions for different damping coefficients.

4. Non-linear analysis

The derived equations of motion and determined region of stability enable one to proceed with a non-linear analysis in order to examine the near-critical behaviour of the system. One of the most important problems to be investigated is to recognise the conditions in which the flutter instability occurs, i.e. whether the self-excited vibration is of a soft or hard type. Expressing the problem in mathematical terms, we deal with Hopf's bifurcation as the trivial static equilibrium position evolves into a periodic solution. Having found such a solution, describing in fact a limit cycle, it is possible to evaluate its orbital stability. This allows one to predict the properties of the bifurcating vibration and determine if it is super- or subcritical. In the latter case the system is threatened with a catastrophic loss of the stability as a slight disturbance, even below the critical threshold could lead to a sudden jump of the vibration amplitude onto the nearest stable limit cycle placed far from the unstable equilibrium position. In order to answer the question in which conditions such a situation could happen it is necessary to construct a bifurcating solution, where the active bifurcation parameters will be the follower load and rotation speed. The approach by Iooss and Joseph (1980) is incorporated into the analysis.

Rewrite the equation of motion, see Eq. (9), in the following form:

$$\dot{\mathbf{w}} = \mathbf{f}(\mathbf{w}, \lambda) \tag{10}$$

and predict the periodic bifurcating solution in the form:

$$\mathbf{w} = \sum_{n=1}^{\infty} \frac{\varepsilon^n}{n!} \mathbf{w}_n(\Phi t) \tag{11}$$

The bifurcating solution is based on $2\pi n$-periodic functions $\mathbf{w}_n$ of the frequency Φ_n expressed in term of a power series with respect to ε as well:

$$\Phi(\varepsilon) = \Phi_0 + \sum_{n=1}^{\infty} \frac{\varepsilon^n}{n!} \Phi_n \tag{12}$$

Analogously, the bifurcation parameter λ (μ or ω):

$$\lambda(\varepsilon) = \lambda_{\mathrm{cr}} + \sum_{n=1}^{\infty} \frac{\varepsilon^n}{n!} \lambda_n \tag{13}$$

From Eq. (12) the reciprocal function $\varepsilon = \varepsilon(\ldots \lambda_n \ldots)$ can be found for a small-degree approximation and coupled with Eq. (11) in order to derive the direct relationship between the bifurcating solution and parameter near the critical threshold λ_{cr}.

Now, take into account the series given by Eqs. (10)–(12) truncated at the second terms:

$$\begin{aligned} &\mathbf{w}(\Phi t, \varepsilon) = \varepsilon \mathbf{w}_1 + \tfrac{1}{2}\varepsilon^2 \mathbf{w}_2 \\ &\Phi = \Phi_0 + \tfrac{1}{2}\varepsilon^2 \Phi_2 2 \\ &\lambda = \lambda_{\mathrm{cr}} + \tfrac{1}{2}\varepsilon^2 \lambda_2 \end{aligned} \tag{14}$$

as it can be proved that for any odd number of n the coefficients Φ_n and λ_n vanish, see Iooss and Joseph (1980). Now, the bifurcating solution assumes the form:

$$\mathbf{w}\{\Phi(\lambda)t\} = \mathbf{w}_1 \sqrt{2\frac{\lambda - \lambda_{\mathrm{cr}}}{\lambda_2}} + \mathbf{w}_2 \frac{\lambda - \lambda_{\mathrm{cr}}}{\lambda_2} \tag{15}$$

where

$$\mathbf{w}_1 = 2\varepsilon \mathrm{Re}\{\mathbf{q}\exp(\mathrm{i}\Phi t)\}, \quad \mathbf{w}_2 = \mathbf{0} \tag{16}$$

as $\mathbf{w}_2$ disappears because of the lack of even-order terms in the equations of motion Eq. (9), see also Eq. (1). The vector $\mathbf{q}$ corresponds to the following eigenproblem:

$$\{\mathbf{A}(\lambda_{\mathrm{cr}}) - r\mathbf{I}\}\mathbf{q} = \mathbf{0} \tag{17}$$

Presented in Eq. (14) coefficients λ_2 and Φ_2 are

$$\lambda_2 = -\frac{\mathrm{Re}\{\Psi_2\}}{3\xi}, \quad \Phi_2 = \lambda_2 \eta + \tfrac{1}{3}\mathrm{Im}\{\Psi_2\} \tag{18}$$

where

$$\xi = \frac{\mathrm{d}}{\mathrm{d}\lambda}(\mathrm{Re}\{r_{\mathrm{m}}(\lambda_{\mathrm{cr}})\}), \quad \eta = \frac{\mathrm{d}}{\mathrm{d}\lambda}(\mathrm{Im}\{r_{\mathrm{m}}(\lambda_{\mathrm{cr}})\}) \tag{19}$$

and

$$\Psi_2 = 3\sum_{i=1}^{8}\sum_{j=1}^{8}\sum_{k=1}^{8}\sum_{l=1}^{8} \frac{\partial f_i(\mathbf{w}, \lambda_{\mathrm{cr}})}{\partial u_j \partial u_k \partial u_l} \bar{q}_i^* q_j q_k \bar{q}_l \tag{20}$$

where the vector $\mathbf{q}^*$ is an eigenvector corresponding to the following adjoint eigenproblem:

$$\{\mathbf{A}^{\mathrm{T}}(\lambda_{\mathrm{cr}}) - \bar{r}\mathbf{I}\}\mathbf{q}^* = \mathbf{0} \tag{21}$$

For uniqueness, the vectors $\mathbf{q}$ and $\mathbf{q}^*$ satisfy the orthonormalisation conditions that imply

$$\langle \mathbf{q}, \mathbf{q}^* \rangle \geqslant \sum_{i=1}^{8} q_i \bar{q}_i^* = 1, \quad \langle \mathbf{q}, \bar{\mathbf{q}}^* \rangle \geqslant \sum_{i=1}^{8} q_i q_i^* = 0 \tag{22}$$

Subsequently, the thus obtained bifurcating solution must be examined with respect to its stability, which depends on the sign of Floquet's exponent defined as

$$\sigma(\varepsilon) = -\xi \lambda_2 \varepsilon^2 + \mathrm{O}(\varepsilon^4) \tag{23}$$

where $\mathrm{O}(\varepsilon^4)$ are negligible terms of higher orders of ε. The trivial solution $\mathbf{w} = \mathbf{0}$ bifurcates onto an orbitally stable limit cycle (supercritical bifurcation) when $\sigma > 0$ or unstable (subcritical bifurcation) if $\sigma < 0$.

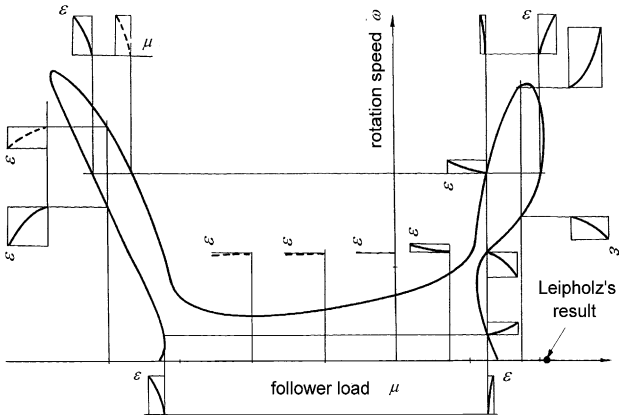

Fig. 6. Near-critical behaviour of the bifurcating solution in the entire area of the stability boundary.

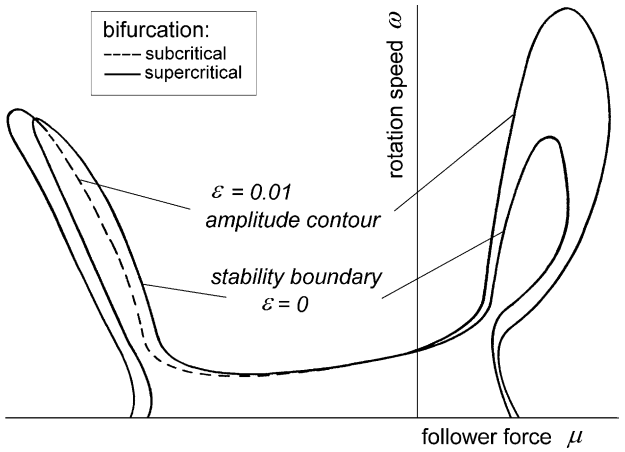

Fig. 7. Evolution of the stability contours for increasing amplitude of the limit cycle.

Some selected results of the bifurcation analysis are presented in Figs. 6 and 7. Bifurcation diagrams depicting the non-critical self-excited vibration amplitude ε around several points lying on the stability boundary are shown in Fig. 6. The parabolic evolutions of ε are shown in the form of cross-sections in the direction of either follower load or rotation speed. As can be seen an appearance of the disadvantageous subcritical bifurcation is possible for compressive follower loads (dashed lines), however certain combinations of μ and ε may exclude such a dangerous response. Fig. 7 presents the evolution of the stability region allowing for increasing amplitude of the sprung-up self-excitation. Expectedly, the subcritical bifurcation occurs for negative μ only.

5. Piezoelectric actuation of the rotating shaft

Recent developments in the field of smart structures and the coming of active composites into being have opened new possibilities to the control of rotating shafts. Composite shafts, due to low specific weight,

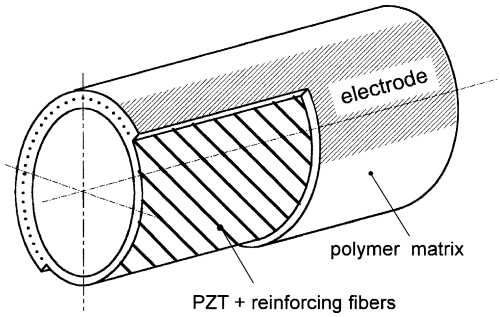

Fig. 8. Laminated column with active fibres.

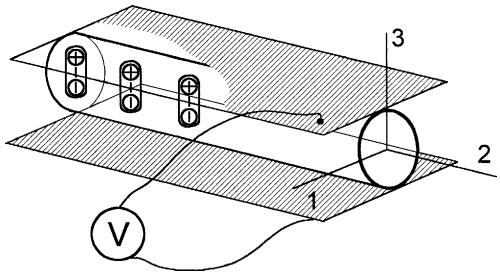

Fig. 9. Single piezoelectric fibre.

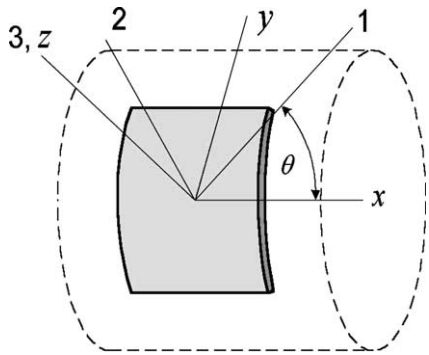

Fig. 10. Sensor layer attached to a shell-like structure.

anisotropic properties, and excellent torsional stiffness are very competitive materials with respect to their traditional steel counterparts. The application of active piezoelectric fibres make them competitive even more.

In this section fundamentals of active control of rotating shafts made of smart laminates containing piezoelectric fibres are discussed in detail. For this purpose assume that the rotating column is a symmetrically laminated composite with embedded transversely poled piezoceramic fibres which can be arbitrarily angle plied together with the reinforcing fibres. Between each lamina there is a set of circumferentially separated actuator electrodes in the form of rectangular patches glued along the column axis. A schematic of the composite column and some of its elements are shown in Figs. 8 and 9.

Before examining the efficiency of the actuation system, check the applicability of light PVDF polymers for sensing the bending vibration that threatens the considered rotating column. The choice of PVDF is due to its distinguished advantages, which are wide frequency range, vast dynamic range, high elasticity and conformability, good voltage output, high dielectric strength withstanding strong 75 V/μm fields, where most piezoceramics fail, and relatively low material and fabrication costs. Piezoelectric films can be cut and glued with commercial adhesives. Many conductive electrode coatings are available in the market.

Consider, in general, a single PVDF ring-shaped thin layer having the anisotropy axes oriented as shown in Fig. 10. The piezoelectric effect is described by the following constitutive equation (in principal anisotropy axes), see Nye (1985):

$$D_i = d_{ij}\sigma_j + \epsilon_{ij}E_j \tag{24}$$

where D_i is the dielectric displacement, d_{ij} are the coefficients of the electromechanical coupling, σ_j is the mechanical stress, ϵ_{ij} are the dielectric permittivity coefficients, E_j is the electric field vector. Assuming the pure direct mechanical-to-electrical conversion effect (excluding presence of any additional electric fields: $\mathbf{E} = \mathbf{0}$) one writes down:

$$D_i = d_{ij}\sigma_j \tag{25}$$

In a more explicit form the shape of the electromechanical coupling matrix can be observed. The lack of natural shear coefficients is worth mentioning, see Damjanovič and Newnham (1992):

$$\begin{bmatrix} D_1 \\ D_2 \\ D_3 \end{bmatrix} = \begin{bmatrix} 0 & 0 & 0 & 0 & 0 & 0 \\ 0 & 0 & 0 & 0 & 0 & 0 \\ d_{31} & d_{32} & d_{33} & 0 & 0 & 0 \end{bmatrix} \begin{bmatrix} \sigma_1 \\ \sigma_2 \\ \sigma_3 \\ \sigma_4 \\ \sigma_5 \\ \sigma_6 \end{bmatrix} \tag{26}$$

For a thin layer (in-plane stress–strain state: $\sigma_3, \sigma_4, \sigma_5 = 0$):

$$\begin{bmatrix} D_1 \\ D_2 \\ D_3 \end{bmatrix} = \begin{bmatrix} 0 & 0 & 0 \\ 0 & 0 & 0 \\ d_{31} & d_{32} & 0 \end{bmatrix} \begin{bmatrix} \sigma_1 \\ \sigma_2 \\ \sigma_3 \end{bmatrix}, \quad \mathbf{D} = \mathbf{d}\boldsymbol{\sigma} \tag{27}$$

Transform now the co-ordinate system $(1,2,3)$ into (x,y,z) by rotation around the third axis $3 \equiv z$ by θ.

$$\bar{\mathbf{D}} = \bar{\mathbf{d}}\bar{\boldsymbol{\sigma}}, \quad \bar{\boldsymbol{\sigma}} = [\sigma_x, \sigma_y, \tau_{xy}]^{\mathrm{T}} \tag{28}$$

where the overbars are relative to the rotated co-ordinate system:

$$\bar{\mathbf{d}} = \mathbf{T}\mathbf{d}\mathbf{T}^{-1}, \quad \text{where } \mathbf{T} = \begin{bmatrix} \cos^2\theta & \sin^2\theta & \sin 2\theta \\ \sin^2\theta & \cos^2\theta & -\sin 2\theta \\ -\frac{1}{2}\sin 2\theta & \frac{1}{2}\sin 2\theta & \cos 2\theta \end{bmatrix} \tag{29}$$

Moreover,

$$\bar{\boldsymbol{\sigma}} = \bar{\mathbf{Q}}\bar{\boldsymbol{\varepsilon}} \Rightarrow \bar{\mathbf{D}} = \bar{\mathbf{d}}\bar{\mathbf{Q}}\bar{\boldsymbol{\varepsilon}}, \quad \bar{\boldsymbol{\varepsilon}} = [\varepsilon_x, \varepsilon_y, \tfrac{1}{2}\gamma_{xy}]^{\mathrm{T}} \tag{30}$$

where $\bar{\mathbf{Q}} = \mathbf{T}\mathbf{Q}\mathbf{T}^{-1}$, which entails $\bar{\mathbf{D}} = \mathbf{T}\mathbf{d}\mathbf{T}^{-1}\mathbf{T}\mathbf{Q}\mathbf{T}^{-1}\bar{\boldsymbol{\varepsilon}} = \mathbf{T}\mathbf{d}\mathbf{Q}\mathbf{T}^{-1}\bar{\boldsymbol{\varepsilon}}$. As PVDFs are poled in the third direction the electrodes must be attached to the normal surfaces. Therefore, the dielectric displacement (and resulting charge) is of the greatest interest:

$$\bar{D}_3 = D_3 = D_z = \left\{\mathbf{T}\mathbf{d}\mathbf{Q}\mathbf{T}^{-1}\right\}_3 \bar{\boldsymbol{\varepsilon}} = [\Delta_1, \Delta_2, \Delta_3] \cdot [\varepsilon_x, \varepsilon_y, \tfrac{1}{2}\gamma_{xy}]^{\mathrm{T}} \tag{31}$$

A single PVDF sensor patch is glued to the surface to each structure shown in Fig. 11.

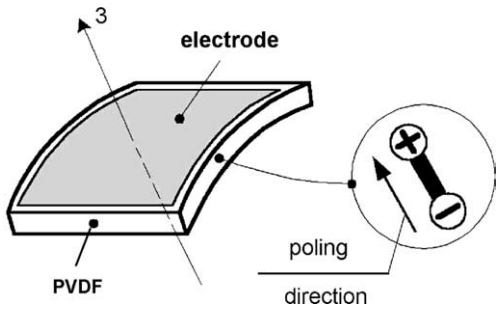

Fig. 11. Polarisation of PVDFs.

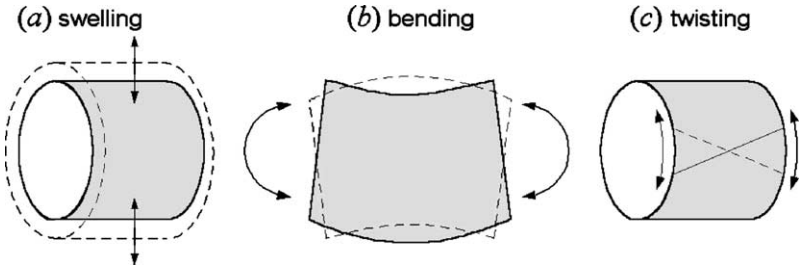

Fig. 12. Measured vibration modes.

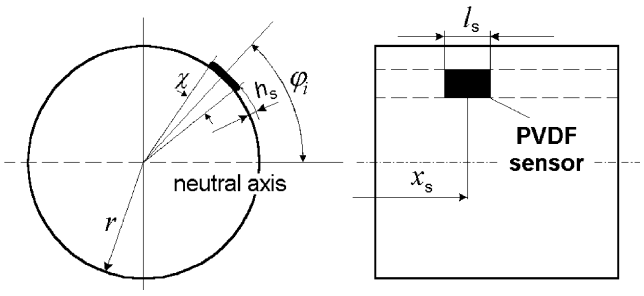

Fig. 13. Model of the sensors for measuring bending modes.

The structure can be subject to a combination of the following vibration modes: (a) transverse vibration due to radial motion (pure swelling in the radial direction), (b) transverse vibration due to bending, (c) torsional vibration (twisting)—see Fig. 12. Find now, how effective can be the PVDF sensor in measuring each of the indicated vibration types:

$$U_S = \frac{q_3}{S} = \frac{q_3 h_s}{\epsilon_s S} = \frac{q_3 h_s}{2\pi\epsilon_s r l_s} \tag{32}$$

Let the sensor be a small rectangular patch bonded to the host structure as shown in Fig. 13. This time (pure bending) the strain vector assumes the form: $\bar{\boldsymbol{\varepsilon}} = [\varepsilon_x, 0, 0]$, and the dielectric displacement in the third (z) axis is

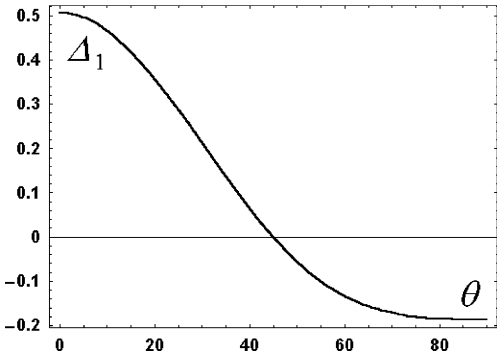

Fig. 14. Efficiency of voltage generation for bending vibration modes vs. orientation of the PVDF sensing patch.

$$D_3 = [\Delta_1, \Delta_2, \Delta_3] \begin{bmatrix} \varepsilon_x \\ 0 \\ 0 \end{bmatrix} = \Delta_1 \varepsilon_x \tag{33}$$

The electric charge and the resulting voltage will be

$$q_3 = \int_A D_3 \, \mathrm{d}A = \Delta_1 r^2 \int_{x_s-(l_s/2)}^{x_s+(l_s/2)} \kappa(x) \mathrm{d}x \int_{\varphi_i-(\chi/2)}^{\varphi_i+(\chi/2)} \sin\varphi \, \mathrm{d}\varphi \tag{34}$$

where

$$\Delta_1 = [\sin^2\theta(d_{32} + \nu_{12} d_{31}) + \cos^2\theta(d_{31} + \nu_{12} d_{32})] \frac{Y_s \cos 2\theta}{1 - \nu_{12}^2} \tag{35}$$

The term Δ_1 strongly depends on the geometric configuration of the attached sensor. This dependence is shown in Fig. 14.

$$U_S = \frac{q_3}{C} = \frac{\Delta_1 h_s r}{\epsilon_s \chi l_s} \int_{x_s-(l_s/2)}^{x_s+(l_s/2)} \kappa(x) \, \mathrm{d}x \left[\cos\left(\varphi_i - \frac{\chi}{2}\right) - \cos\left(\varphi_i + \frac{\chi}{2}\right) \right] \tag{36}$$

where κ denotes the curvature: $\kappa = \partial^2 w / \partial x^2$, the substitution of which entails

$$U_S = \frac{\Delta_1 h_s r}{\epsilon_s \chi l_s} \left[\frac{\partial w\left(x_s + \frac{l_s}{2}\right)}{\partial x} - \frac{\partial w\left(x_s - \frac{l_s}{2}\right)}{\partial x} \right] \cdot 2 \sin\varphi_i \sin\frac{\chi}{2} \tag{37}$$

As can be seen the produced voltage is directly proportional to the difference between the slopes at the beginning and ending points of the sensor patch. For very small sensor elements (both in the radial and longitudinal directions), Eq. (37) can be rewritten as follows:

$$\begin{aligned} U_S &= \lim_{\substack{l_s \to 0 \\ \chi \to 0}} U_S(l_s, \chi) = 2 \frac{\Delta_1 h_s r}{\epsilon_s} \sin\varphi_i \lim_{l_s \to 0} \frac{\frac{\partial w\left(x_s + \frac{l_s}{2}\right)}{\partial x} - \frac{\partial w\left(x_s - \frac{l_s}{2}\right)}{\partial x}}{l_s} \lim_{\chi \to 0} \frac{\sin\frac{\chi}{2}}{\chi} \\ &= \frac{\Delta_1 h_s r}{\epsilon_s} \frac{\partial^2 w(x_s)}{\partial x^2} \sin\varphi_i \end{aligned} \tag{38}$$

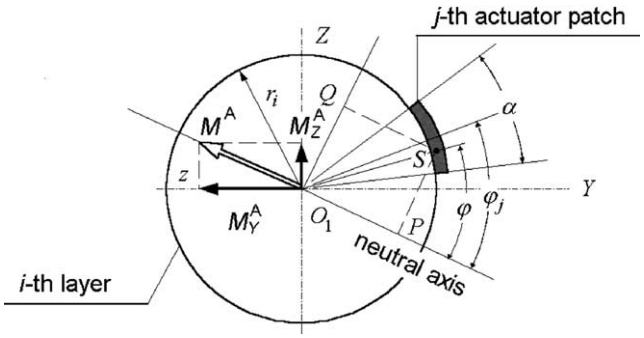

Fig. 15. Actuator patch controlling a part of the piezoelectric fibres.

Consider now a single layer of a composite shaft with an electrode covering a single bunch of piezoelectric fibres embedded right beneath the electrode, see Fig. 15. The bending moment M_{ij}^{A} produced by the jth actuator in the ith composite layer is

$$M_{ij}^{\mathrm{A}} = \int_{A_{ij}} \sigma_x^{\mathrm{A}} PS \,\mathrm{d}A = \int_{A_{ij}} \Xi_\sigma E_{ij} r \sin\varphi \,\mathrm{d}A \tag{39}$$

where E_{ij} is the electric field applied to the jth electrode on the ith layer, and Ξ_σ is a piezoelectric constant describing the material and electromechanical properties as well as geometric parameters (including the lamination angle θ) of the active lamina.

The integration area A_{ij} appearing in (39) can be described as follows:

$$A_{ij} = \left\{ (r,\varphi) : r_i \leqslant r \leqslant r_i + \frac{h}{N}, \varphi_j - \frac{\alpha}{2} \leqslant \varphi \leqslant \varphi_j + \frac{\alpha}{2} \right\} \tag{40}$$

where r_i is the inside radius of the ith layer, h is the thickness of the laminate shaft, N is the number of layers, φ_j is the current angular position of the middle point of the jth electrode patch (actuator), α is the angular width of the electrode (assumed the same for every actuator). Hence,

$$M_{ij}^{\mathrm{A}} = \Xi_\sigma E_{ij} \int_{r_i}^{r_i+(h/N)} r^2 \,\mathrm{d}r \int_{\varphi_j-(\alpha/2)}^{\varphi_j+(\alpha/2)} \sin\varphi \,\mathrm{d}\varphi \tag{41}$$

if the electric field and composition of the embedded piezoelectric fibres are homogeneous. Assuming that $h/r \ll 1$:

$$M_{ij}^{\mathrm{A}} = 2\Xi_\sigma E_{ij} r_i^2 \frac{h}{N} \sin\varphi_j \sin\frac{\alpha}{2} \tag{42}$$

The voltage measured by a single piezoelectric (e.g. PVDF) sensor associated with jth actuator electrode on the ith composite layer would be

$$U_{\mathrm{S}ij} = \frac{\Delta_1 r_i h_{\mathrm{s}}}{\epsilon_{\mathrm{s}}} \frac{\partial^2 w(x_{\mathrm{s}})}{\partial x^2} \sin\varphi_j \tag{43}$$

where h_{s} is the sensor thickness, ϵ_{s} is its dielectric permittivity, x_{s} is its location along the column axis.

Assuming the control strategy as a simple velocity feedback, one notes

$$U_{\mathrm{A}ij} = \kappa \frac{\mathrm{d}U_{\mathrm{S}ij}}{\mathrm{d}t} \tag{44}$$

It should be noted that the above strategy, however linear by principle, strongly affects the non-linear response of the system as it creates new dynamic conditions in which the eventual limit cycle originates.

Thus the linear control may change the quality of the bifurcation process that takes place at the criticality, and possibly change its general character (e.g. convert harsh subcritical bifurcation into a smooth one, supercritical).

Knowing that $E_{ij} = U_{\mathrm{A}ij}/(h/N)$ and $\mathrm{d}\sin\varphi_j/\mathrm{d}t = \omega\cos\varphi_j$, the electric field controlling the ijth actuator will be

$$E_{ij} = \frac{N\Delta_1 r_i h_\mathrm{s}}{h\epsilon_\mathrm{s}}\kappa\frac{\mathrm{d}}{\mathrm{d}t}\left(\frac{\partial^2 w(x_\mathrm{s},t)}{\partial x^2}\sin\varphi_j\right) \tag{45}$$

and, finally, the actuating moment:

$$M^\mathrm{A}_{ij} = 2\kappa\Xi_\sigma\frac{\Delta_1 r_i^3 h_\mathrm{s}}{\epsilon_\mathrm{s}}\sin\varphi_j\sin\frac{\alpha}{2}\left(\frac{\partial^3 w(x_\mathrm{s},t)}{\partial x^2\partial t}\sin\varphi_j + \omega\frac{\partial^2 w(x_\mathrm{s},t)}{\partial x^2}\cos\varphi_j\right) \tag{46}$$

The resultant moment is

$$M^\mathrm{A} = \sum_{i=1}^{N}\sum_{j=1}^{n} M^\mathrm{A}_{ij} \tag{47}$$

where N is the number of layers the composite shaft is made of, n is the number of electrode patches (actuators) along the perimeter of a single layer. Hence,

$$M^\mathrm{A}_{ij} = 2\kappa\Xi_\sigma\frac{\Delta_1 r_i^3 h_\mathrm{s}}{\epsilon_\mathrm{s}}\sin\frac{\alpha}{2}\left(\frac{\partial^3 w(x_\mathrm{s},t)}{\partial x^2\partial t}\sum_{i=1}^{N} r_i^3\sum_{j=1}^{n}\sin^2\varphi_j + \omega\frac{\partial^2 w(x_\mathrm{s},t)}{\partial x^2}\sum_{i=1}^{N} r_i^3\sum_{j=1}^{n}\sin\varphi_j\cos\varphi_j\right) \tag{48}$$

Let r denote the average radius of the thin-walled shaft structure, thus

$$r_i = r + h\frac{2\mathrm{i} - N}{N} = r\left[1 + \frac{h}{2rN}(2\mathrm{i} - N)\right] \tag{49}$$

Since $h/r \ll 1$ (and additionally divided by $2N > 1$) it is reasonable to assume $r_i = r$, which entails

$$\sum_{i=1}^{N}\left(r + h\frac{2\mathrm{i} - N}{N}\right)^3 \approx Nr^3 \tag{50}$$

Have a closer look now at the sums in (48) involving the expressions of the angular position φ_j. Note, that the angular distance between the jth and $j+1$th electrode patch is $\varphi_{j+1} - \varphi_j = 2\pi/n$. Denoting the position of the first patch by $\varphi_1 = \varphi$ one finds the locations of the subsequent electrodes to be $\varphi_j = \varphi + 2\pi j/n$. Studying the properties of the sums in (48) one can state:

$$\sum_{j=1}^{n}\sin^2\varphi_j = \sum_{j=1}^{n}\sin^2\left(\varphi_j + j\frac{2\pi}{n}\right) = \begin{cases}\sin^2\varphi & \text{for } n = 1\\ 2\sin^2\varphi & \text{for } n = 2\\ \dfrac{n}{2} & \text{for } n \geqslant 3\end{cases} \tag{51}$$

and

$$\sum_{j=1}^{n}\sin\varphi_j\cos\varphi_j = \tfrac{1}{2}\sum_{j=1}^{n}\sin 2\left(\varphi_j + j\frac{2\pi}{n}\right) = \begin{cases}\dfrac{1}{2}\sin 2\varphi & \text{for } n = 1\\ \sin 2\varphi & \text{for } n = 2\\ 0 & \text{for } n \geqslant 3\end{cases} \tag{52}$$

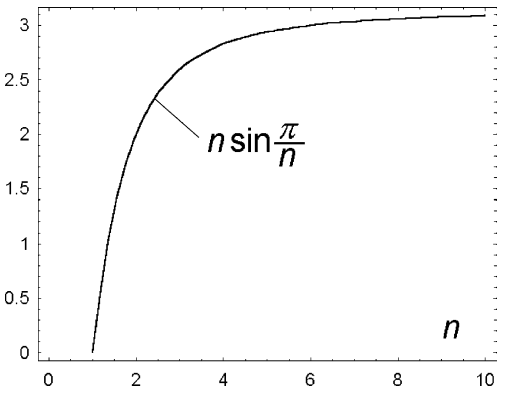

Fig. 16. Actuating moment vs. number of electrode patches.

It is a very important conclusion that the application of three or more electrode patches ensures the generation of a *constant* bending moment, i.e. a non-pulsating one, despite the discrete distribution of the patches along the perimeter and rotary motion of the shaft. Finally,

$$M^{\mathrm{A}} = \kappa \Xi_{\sigma} \frac{N \Delta_1 r_i^3 h_{\mathrm{s}}}{\epsilon_{\mathrm{s}}} \frac{\partial^3 w(x_{\mathrm{s}}, t)}{\partial x^2 \partial t} n \sin \frac{\pi}{n} \tag{53}$$

where $\sin(\alpha/2)$ has been replaced with $\sin(\pi/n)$, which holds true for negligible gaps separating and insulating the electrode patches.

Except for the material and structural parameters, the actuating moment is directly proportional to the curvature and its first time derivative. There appears yet another parameter responsible for the magnitude of M^{A}—the number n of the actuator electrodes per each layer. The question is to what extent M^{A} depends on n (what is the limit value of M^{A}, what is the minimum one?). To answer this, draw a diagram of the function $n\sin(\pi/n)$ standing in (53). The moment M^{A} is proportional to this function, see Fig. 16. The maximum bending moment produced by the piezoelectric fibres is strictly related with the following limit:

$$\lim_{n\to\infty} n \sin \frac{\pi}{n} = \pi \tag{54}$$

It is clearly seen (Fig. 16) that an infinite increase in the number of electrode patches is useless. Fine segmentation of the electrodes yields incommensurable results with a degree of unavoidable technical

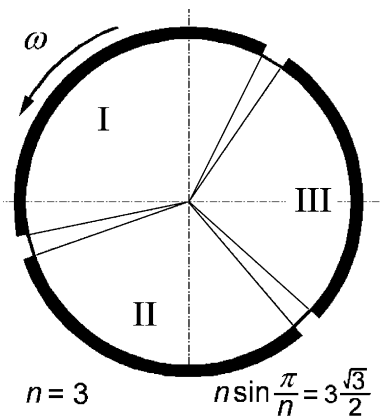

Fig. 17. The least number of electrodes generating a constant bending moment.

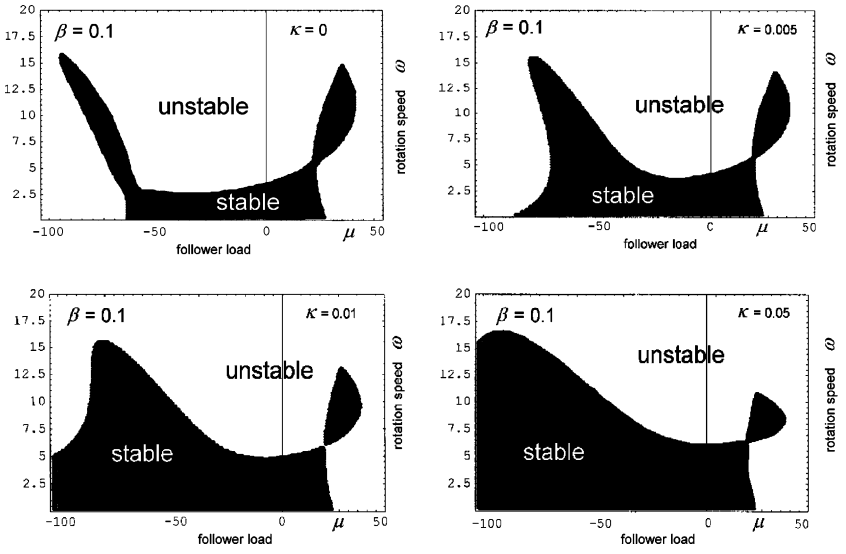

Fig. 18. Evolution of the stability region vs. gain κ in the active control system.

complication of the control system. It is preferable to use the least possible number of actuators along the perimeter in achieving the desired effect, i.e. the smooth operation of the stabilising system (constant counter-bending). This amounts to the incorporation of a three-electrode control set, see Fig. 17.

6. Effect of active stabilisation

Having decomposed the obtained stabilising moment M^{A}, see (53), into M_Y^{A} and M_Z^{A} components, and substituting them into equations of motion (1) and (2), one can proceed with the stability analysis once again in the same way as it was done in Section 3. By tracking the eigenvalues of the matrix of the linearised equations of motion (this time with non-zero terms M_Y^{A} and M_Z^{A}) in various operating conditions, i.e. different combinations of the rotation speed and follower load, one can determine regions of stable and unstable working of the shaft. Exemplary results are shown in Fig. 18.

First of the diagram ($\kappa = 0$) shows combinations of ω and μ corresponding to the stable and unstable operation of the rotating column without active control (behaviour of an ordinary column). The other depict evolution of the stability domain for increasing gain factors κ. It is clearly visible that the application of active control leads to the widening of the stability domain. This effect is particularly pronounced for moderate follower loads. For instance, the relative growth of the critical speed in the range of its maximum sensitivity ($-50 > \mu > -75$) reaches even 400%. Further increase of ω_{cr} is not allowed because of the breakdown voltage limit which equals 75 kV/mm in PZT piezoceramics. In the numerical experiments the control voltage applied to the actuator fibres did not exceed 10% of the breakdown value (roughly 200 V for fibres 30 μm in diameter).

7. Concluding remarks

The paper is concerned with a rotating cantilever column (slender shaft) subject to a tip-concentrated follower load and actively stabilised by piezoelectric elements. The shaft is made of an active laminate—the

piezoelectric fibre composite. A velocity feedback is assumed in the system of active stabilisation. Analysis proves that rotation and follower load contradict each other eventually stabilising the system. Unexpectedly, the stability region appears to be a concave set. Application of active stabilisation yields desirable effects as the area of safe working enlarges in general. It turns out that shafts undergoing compression are particularly sensitive to such a stabilisation method, however in the case on tensile loads the approach becomes ineffective—the system can be stabilised with respect to e.g. follower load but at the cost of angular velocity, the critical threshold of which drops.

Acknowledgement

This work has been done as a part of the research work within Grant No. 7 T07C 024 18 supported by the State Committee for Scientific Research in Poland which is gratefully acknowledged by the authors.

References

Altman, W., Goncalves de Oliveira, M., 1990. Vibration and stability of shell panels with slight internal damping under follower force. Journal of Sound and Vibration 136, 45–50.

Beck, M., 1959. Die Knicklast des einseitig eingespannten, tangential gedrückten Stabes. Zeitschrift für Angewan dte Mathematik und Physik 3, 225.

Bent, A.A., Hagood, N.W., 1997. Piezoelectric fiber composites with interdigitated electrodes. Journal of Intelligent Material Systems and Structures 8 (11), 903–919.

Bent, A.A., Hagood, N.W., Rodgers, J.P., 1995. Anisotropic actuation with piezoelectric fiber composites. Journal of Intelligent Material Systems and Structures 6 (3), 338–349.

Damjanovič, D., Newnham, R.E., 1992. Electrostrictive and piezoelectric materials for actuator applications. Journal of Intelligent Material Structures and Systems 3 (4), 190–208.

De Rosa, M.A., Franciosi, C., 1990. The influence of an intermediate support on the stability behaviour of cantilever beams subjected to follower forces. Journal of Sound and Vibration 137, 107–115.

Iooss, G., Joseph, D.D., 1980. Elementary stability and bifurcation theory. Springer-Verlag, New York.

Kurnik, W., Pękalak, M., 1992. Stability and bifurcation analysis of the non-linear damped Leipholz column. Journal of Sound and Vibration 152 (2), 285–294.

Kurnik, W., Przybyłowicz, P.M., 1995. Nonlinear behavior of the Leipholz column actively stabilized by piezoelements. In: Proceedings of the International Symposium on Active Control of Sound and Vibration ACTIVE '95. Newport Beach.

Kurnik, W., Przybyłowicz, P.M., 2001. Stability of rotating cantilever columns under follower loads. In: Proceedings of the IX International Symposium on Dynamic Problems of Mechanics DINAME. Florianópolis, Santa Catarina, Brazil.

Leipholz, H.H.E., 1972. On the sufficiency of the energy criterion for the stability of certain nonconservative systems of the follower type. Journal of Applied Mechanics 39, 717–722.

Leipholz, H.H.E., 1980. Stability of Elastic Systems. Sijthoff & Noordhoff, Netherlands.

Newnham, R.E., Bowen, K.A., Klicker, K.A., Cross, L.E., 1980. Composite piezoelectric transducers. Material Engineering 2, 93–106.

Nye, J.F., 1985. Physical Properties of Crystals. Clarendon, Oxford.

Païdoussis, M.P., Semler, C., 1993. Nonlinear and chaotic oscillations of a constrained cantilevered pipe conveying fluid. Nonlinear Dynamics 4 (6), 655–670.

Sporn, D., Schoencker, A., 1999. Composites with piezoelectric thin fibers—first evidence of piezoelectric behaviour. Material Resource Innovations 2, 303–308.